Cooperative mechanisms of fast-ion conduction in gallium-based oxides with tetrahedral moieties

EMMA KENDRICK[1], JOHN KENDRICK[2], KEVIN S. KNIGHT[3,4], M. SAIFUL ISLAM[5]* AND PETER R. SLATER[1]*

[1]Materials Chemistry, UniS Materials Institute, University of Surrey, Guildford GU2 7XH, UK
[2]Institute of Pharmaceutical Innovation, University of Bradford, Bradford, BD7 1DP, UK
[3]ISIS Science Diffraction & Muon Division, CCLRC Rutherford Appleton Laboratory, Chilton, Didcot OX11 0QX, UK
[4]Department of Mineralogy, The Natural History Museum, Cromwell Road, London SW7 5BD, UK
[5]Department of Chemistry, University of Bath, Bath BA2 7AY, UK
*e-mail: m.s.islam@bath.ac.uk; p.slater@surrey.ac.uk

Published online: 21 October 2007; doi:10.1038/nmat2039

The need for greater energy efficiency has garnered increasing support for the use of fuel-cell technology, a prime example being the solid-oxide fuel cell[1,2]. A crucial requirement for such devices is a good ionic (O^{2-} or H^+) conductor as the electrolyte[3,4]. Traditionally, fluorite- and perovskite-type oxides have been targeted[3–6], although there is growing interest in alternative structure types for intermediate-temperature (400–700 °C) solid-oxide fuel cells. In particular, structures containing tetrahedral moieties, such as $La_{1-x}Ca_xMO_{4-x/2}$ (M = Ta, Nb, P) (refs 7,8), $La_{1-x}Ba_{1+x}GaO_{4-x/2}$ (refs 9,10) and $La_{9.33+x}Si_6O_{26+3x/2}$ (ref. 11), have been attracting considerable attention recently. However, an atomic-scale understanding of the conduction mechanisms in these systems is still lacking; such mechanistic detail is important for developing strategies for optimizing the conductivity, as well as identifying next-generation materials. In this context, we report a combined experimental and computational modelling study of the $La_{1-x}Ba_{1+x}GaO_{4-x/2}$ system, which exhibits both proton and oxide-ion conduction[9,10]. Here we show that oxide-ion conduction proceeds via a cooperative 'cog-wheel'-type process involving the breaking and re-forming of Ga_2O_7 units, whereas the rate-limiting step for proton conduction is intra-tetrahedron proton transfer. Both mechanisms are unusual for ceramic oxide materials, and similar cooperative processes may be important in related systems containing tetrahedral moieties.

Research into solid-oxide fuel-cell electrolytes has focused mainly on fluorite or perovskite-type oxides[3–6], which are doped with acceptor ions to introduce oxide-ion vacancies. Oxide-ion conduction then proceeds through oxygen 'jumps' via these vacancy defects. In principle, water may be incorporated into the oxide-ion vacancies according to equation (1), leading to the presence of proton defects, which are present as hydroxyl anions.

$$H_2O + V_o^{\bullet\bullet} + O_o \leftrightarrow 2OH_o^{\bullet} \quad (1)$$

These protonic defects account for the proton conductivity observed in doped $BaCeO_3$, $BaZrO_3$ and related systems, with ion transport involving hopping of lone protons between oxide ions (Grotthuss mechanism)[4,5]. Recently there has been growing interest in the search for other structure types for the next generation of proton-conducting ceramics, with particular attention devoted to materials containing tetrahedral moieties, for example, $Ln_{1-x}A_xMO_{4-x/2}$ (Ln = rare earth; M = Ta, Nb, P) (refs 7,8). Recently we reported high proton and oxide-ion conductivity in $La_{1-x}Ba_{1+x}GaO_{4-x/2}$ (refs 9,10), which also contains a tetrahedral unit (GaO_4). The proton conductivity dominates at temperatures below 700 °C in wet atmospheres, with values as high as 1×10^{-4} S cm^{-1} at 500 °C (refs 9,10).

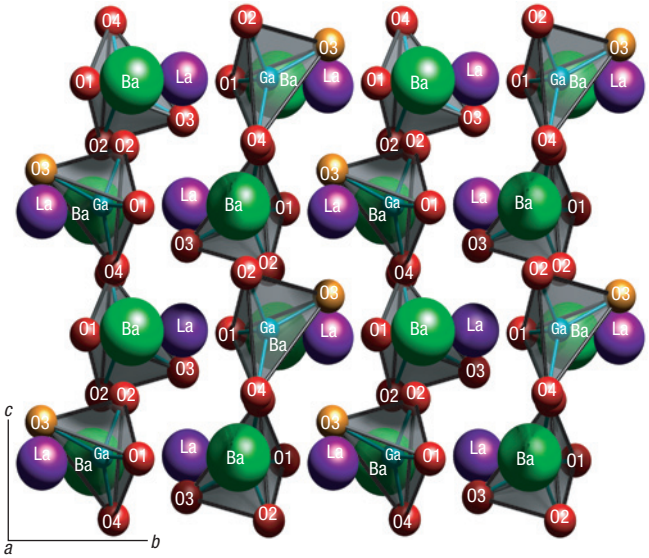

Figure 1 Crystal structure of $LaBaGaO_4$. The structure is unusual in that it contains Ga in a distorted tetrahedral environment.

Despite the growing interest in materials of this type, a detailed understanding of how the oxygen vacancies are accommodated in the structure, and the mechanisms for oxide-ion and proton migration is still clearly lacking. Such mechanistic detail on the atomic level is crucial for a greater understanding of their transport behaviour, which underpins potential applications. This

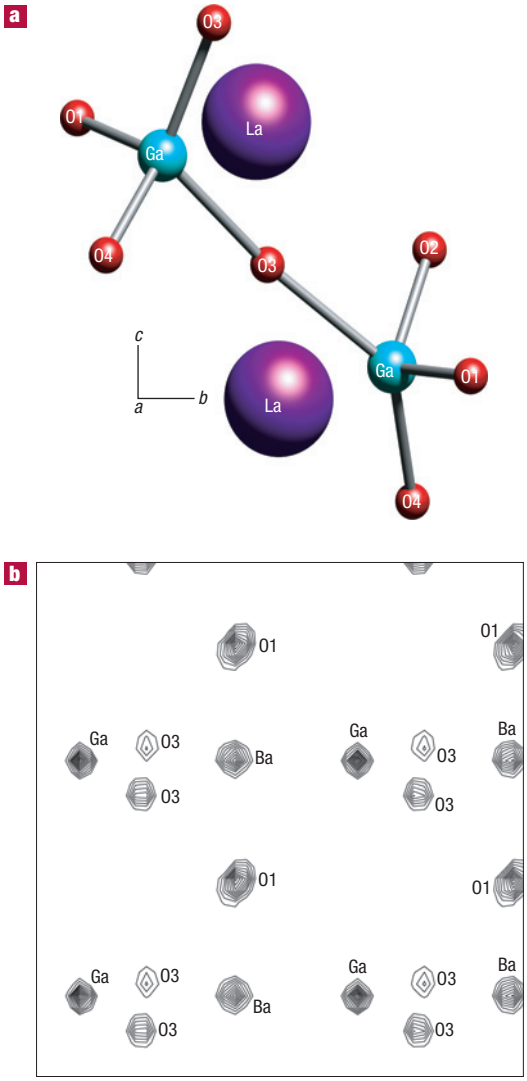

Figure 2 Local structure around an oxide-ion vacancy defect in the $LaBaGaO_4$ system. a, Atomistic modelling reveals considerable local relaxation associated with an oxide-ion vacancy to form a Ga_2O_7 unit. Removal of an oxide ion from one GaO_4 tetrahedron causes a neighbouring tetrahedron to share one of its anions so that both maintain four-fold coordination. This requires slight rotation of both gallium–oxygen moieties. **b**, Fourier map from neutron diffraction data showing ion positions in $La_{0.8}Ba_{1.2}GaO_{3.9}$ at 4 K. Increasing the Ba/La ratio introduces oxide-ion vacancies that cause a split in the O3 positions. The lower density O3 corresponds to the shared anion in the Ga_2O_7 units. Densities were calculated from neutron diffraction results for a slice 2 Å from the unit-cell origin along the *a* axis.

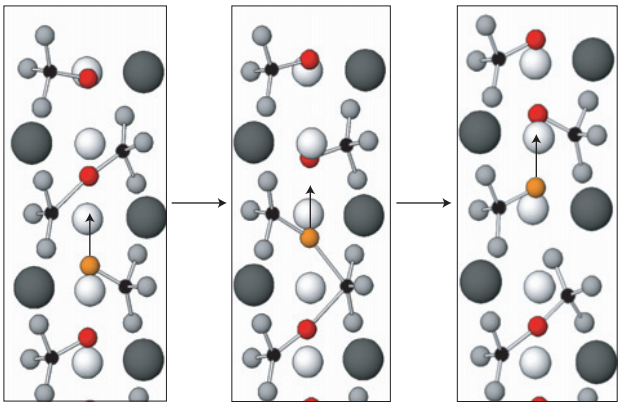

Figure 3 Lowest-energy pathway for oxygen vacancy migration in $La_{1-x}Ba_{1+x}GaO_{4-x/2}$. Snapshots taken from simulations show the microscopic mechanism of oxide-ion migration involving the formation and breaking of Ga_2O_7 units. The transfer of oxide ions between neighbouring tetrahedra enables long-range diffusion to take place. The migrating oxide ions are highlighted, and the 'stick' bonds are drawn to aid the interpretation of the transport mechanism.

study addresses these factors through a powerful multi-technique approach where atomistic potential-based and density-functional theory (DFT) simulation techniques complement and aid the analysis of experimental data.

Figure 1 shows the structure of $LaBaGaO_4$, which contains gallium in a distorted tetrahedral environment and ordered alternating layers of lanthanum and barium. The gallate tetrahedra are clearly seen to be isolated moieties within the lattice. Room-temperature Rietveld refinement of neutron powder diffraction data gave cell parameters of $a = 10.01364(4)$, $b = 7.26536(3)$, $c = 5.90952(2)$ Å (space group $P2_12_12_1$) for the stoichiometric sample, $LaBaGaO_4$; acceptor doping with barium in place of lanthanum to give $La_{0.8}Ba_{1.2}GaO_{3.9}$ resulted in an increase in the cell parameters to $a = 10.06687(8)$, $b = 7.35716(6)$, $c = 5.94336(5)$ Å, owing to the larger ionic radius of Ba^{2+} relative to La^{3+}.

The cell parameters and atomic positions obtained for $LaBaGaO_4$ from the Rietveld refinement were used to develop an atomistic potential model, and as the starting point for quantum mechanical DFT-based calculations. Both computational methods reproduce this complex structure, with good agreement with the experimental data. In particular, both methods successfully reproduced the distorted nature of the GaO_4 tetrahedron, where the O–Ga–O bond angles have values between 98° and 132°. The defect properties of this material were then investigated, enabling detailed analysis of the oxygen vacancy defects and oxygen diffusion pathways, as well as proton incorporation and migration.

Both potential-based and DFT simulations demonstrate that rather than producing three-coordinate Ga units, the oxygen vacancy defects are accommodated by considerable relaxation of a neighbouring GaO_4 unit, resulting in the formation of a Ga_2O_7 group, such that each Ga retains tetrahedral coordination (Fig. 2a). The formation of these Ga_2O_7 defects is a significant finding, and its prediction from the modelling work caused a re-examination of the neutron diffraction data for the 'dry' $La_{0.8}Ba_{1.2}GaO_{3.9}$ sample. Fourier maps were calculated from the neutron diffraction data, and these showed a spread of nuclear density along the *c* axis (Fig. 2b). Furthermore, the best fit to this nuclear density distribution was achieved using a split oxygen (O3) site, which is consistent with the presence of both an isolated GaO_4 tetrahedron and a Ga_2O_7 unit, thereby confirming the modelling predictions. The possibility of this second area of nuclear density being an OH group from small quantities of incorporated water was also considered. Neutron diffraction analyses of two 'wet' $La_{0.8}Ba_{1.2}GaO_{3.9}$ samples treated in H_2O/O_2 and D_2O/O_2 both showed full occupancy of the normal O3 site, with Fourier maps exhibiting no second region of nuclear density, and therefore this OH hypothesis was eliminated (see the Supplementary Information).

The identification of Ga_2O_7 as an important moiety in the accommodation of oxygen vacancies raises key questions concerning how oxide-ion migration may occur in these systems, because at first glance, the formation of such a unit might be

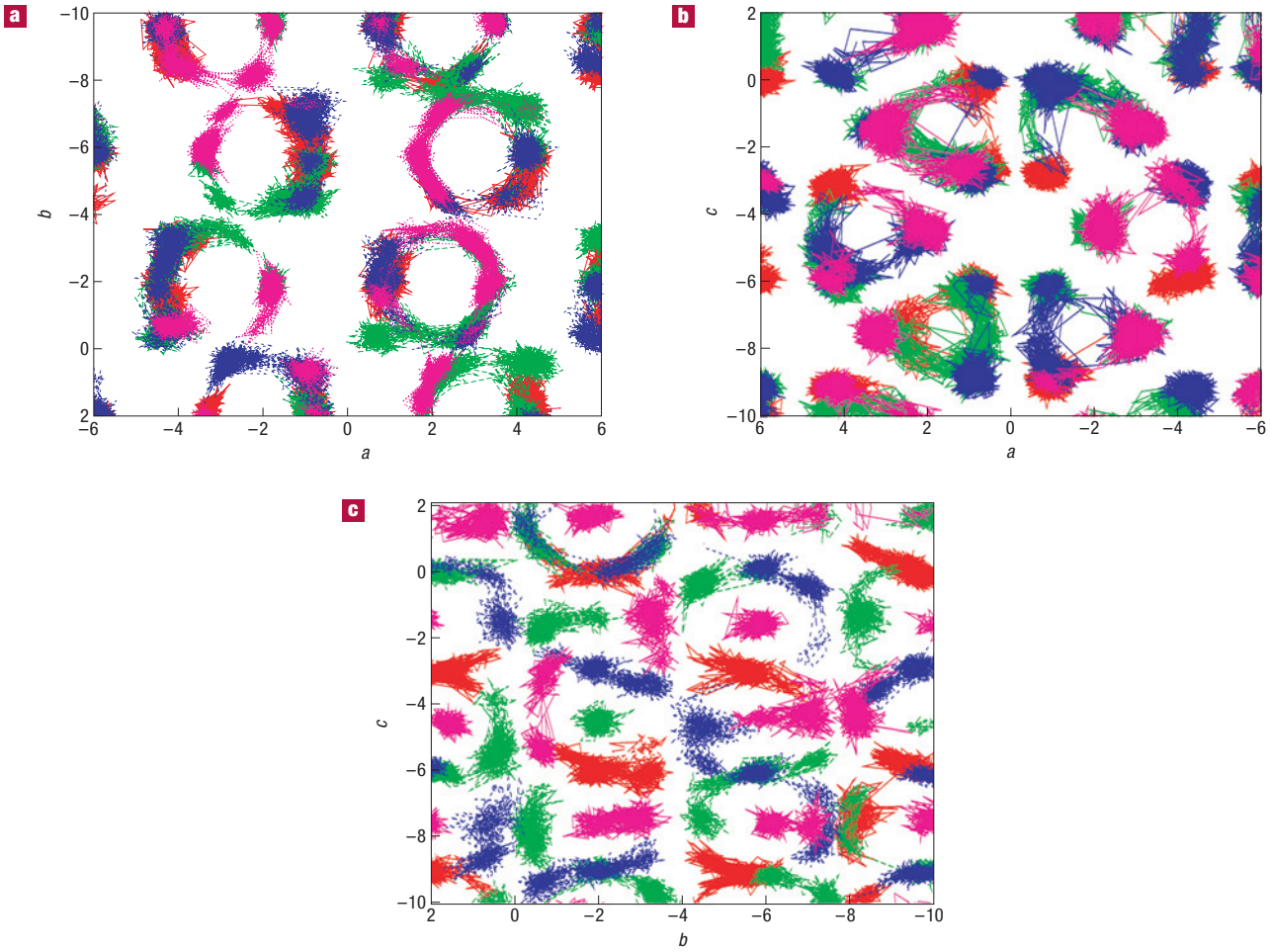

Figure 4 Molecular dynamics simulation trajectories of oxide ions in three mutually perpendicular planes. a, Motion of the anions (red = O1, green = O2, blue = O3, pink = O4) during molecular dynamics simulations reveals that motion in the *ab* plane is mostly the facile rotation of the tetrahedra, and does not contribute significantly to long-range oxide-ion diffusion. **b**,**c**, Motion in the *ac* (**b**) and *bc* (**c**) planes reveal more correlated diffusional features: the interconnected trajectories across the *bc* (**c**) plane reveals that long-range diffusion mostly takes place in this plane, indicating anisotropic migration pathways.

considered as a potential oxide-ion vacancy trapping site, thus limiting oxide-ion migration. Consequently, possible mechanisms for oxygen vacancy migration were investigated.

A series of atomistic potential-based simulations were carried out to investigate several possible pathways for oxide-ion migration. The merit of our simulation approach is that it models local lattice relaxation around the migrating ion and, therefore, the lattice is not treated simply as a rigid lattice of fixed ions. The lowest energy pathway (Fig. 3) was shown to occur via the breaking and re-formation of the Ga_2O_7 units with an oxide-ion migration energy of 0.59 eV. The transfer of oxide ions between neighbouring tetrahedra facilitates long-range diffusion. Thus, rather than inhibiting the conduction process, the Ga_2O_7 units are integral to it.

To explore the mechanistic features of oxide-ion migration more fully, molecular dynamics simulations were carried out on $La_{0.8}Ba_{1.2}GaO_{3.9}$. These revealed significant oxide-ion diffusion, with the data supporting the static lattice calculation results: the diffusion occurs by the breaking and re-formation of Ga_2O_7 units and a similar overall migration activation energy (0.55 eV). The calculated migration energies are comparable to, but lower than, the experimental activation energy[10] (0.83 eV). However, it is worth noting that these calculated values relate to intrinsic migration of oxide-ion vacancies and do not include energy terms from defect association (or trapping) around the acceptor (Ba) dopant. The migration activation energies from both potential-based static lattice and molecular dynamics simulations are lower than the experimental value, which may imply that such defect trapping, as observed in other oxide-ion conductors (refs 3,12), is more significant than effects due to anisotropy.

Extended analysis of the oxygen trajectories over the temperature range 673–1,673 K showed significant rotational contributions from the tetrahedra. Thus, the motion in the *ab* plane is mainly rotation of tetrahedra, whereas an inspection of the plots for the *ac* and *bc* planes shows more diffusional transport features (Fig. 4), with the main direction of diffusion in the *c* direction, in agreement with the static lattice simulations. The trajectory plots show the role of the rotation of the tetrahedra in the diffusion of the oxygen atoms. These results illustrate the isotropic rotational movement of the oxygen atoms around each tetrahedron and the anisotropic diffusion between tetrahedra.

This predicted oxide-ion conduction pathway is unusual and reminiscent of a concerted 'cog-wheel'-type motion, with the effective transfer of oxide-ion vacancies facilitated by Ga_2O_7 defects.

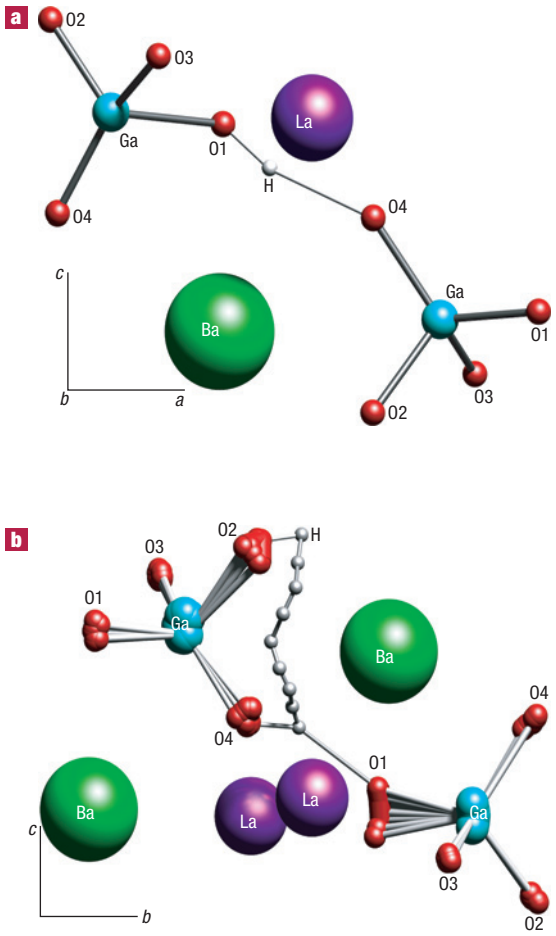

Figure 5 Proton configuration and migration in $LaBaGaO_4$. a, Calculated relaxed configuration of a proton from static lattice simulations. Hydrogen bonding interactions were found between the proton and an oxide ion of a neighbouring GaO_4 tetrahedron. **b**, Proton migration pathway around a GaO_4 tetrahedron from DFT calculations. The proton follows a curved path between two intra-tetrahedral oxide ions probably owing to repulsive interactions with adjacent large cations. There is also significant local ion movement with the O–O separation contracting to about 2.5 Å to facilitate the proton transfer process.

The process requires significant rotation of the Ga_2O_7 and GaO_4 units, suggesting that the structure is relatively flexible and allows facile rotation of these units. In support of this, DFT calculations of rotation of the GaO_4 unit gave a barrier energy of 0.6 eV.

To investigate the location of protons in $La_{1-x}Ba_{1+x}GaO_{4-x/2}$, atomistic (potential-based) and DFT calculations were carried out, with both techniques giving similar energies for proton defects at every oxygen position, indicating a range of possible proton sites. The energy for incorporation of water (equation (1)) is calculated to be favourable, with a magnitude ($E_{(H_2O)} = -0.60$ eV) comparable to the exothermic values obtained experimentally for other proton-conducting oxides[4]. Therefore, as with these other oxides, the defect (and hence conduction) behaviour of the $La_{1-x}Ba_{1+x}GaO_{4-x/2}$ system will be dominated by oxygen vacancies at high temperatures and by protons at low temperatures. This water incorporation leads to the break-up of the Ga_2O_7 units.

$$Ga_2O_7^{8-} + H_2O \rightarrow 2GaO_4H^{4-}$$

Table 1 Activation energies for proton migration around a GaO_4 unit (intra-tetrahedron) and between two adjacent GaO_4 tetrahedra (inter-tetrahedra) determined from DFT calculations.

	E_a (eV)
Intra-tetrahedron	
01 to 03	0.75
02 to 04	0.68
04 to 01	0.55
04 to 02	0.45
Inter-tetrahedra	
01 to 02	0.07
03 to 03	0.07

For each protonic defect, hydrogen bonding was found between the proton and an oxygen atom of a neighbouring GaO_4 tetrahedron (Fig. 5a). The activation energies for proton migration around a GaO_4 unit (intra-tetrahedron migration) and between two adjacent GaO_4 units (inter-tetrahedra migration) were calculated using the DFT nudged elastic band (NEB) method (Table 1). These results show very low inter-tetrahedra migration energies consistent with significant mediation through hydrogen bonding; appreciable ion movement with shorter O–O separations at the barrier state is also found, which helps to facilitate proton transfer (as shown previously in perovskite-type oxides[5]). The calculations suggest that the rate-determining step for long-range proton diffusion is related to intra-tetrahedron migration (Fig. 5b). For such a process, the highest barrier energy is calculated to be 0.75 eV (Table 1). Interestingly, this value is in excellent agreement with an experimentally observed activation energy of 0.76 eV (refs 9,10).

In contrast to the oxide-ion conduction mechanism, which seems to be dominated by correlated diffusion along the direction defined by the Ga_2O_7 units, proton conduction is expected to be isotropic, with the H-bonding-mediated transfer of protons between GaO_4 units within a layer and between layers being equally favourable. Similarities between this system and solid-acid proton conductors such as CsH_2PO_4, which are attracting considerable interest for low-temperature fuel-cell applications, may also need to be explored[13]. For example, in the high-temperature superprotonic phase, CsH_2PO_4 exhibits a large number of potential tetrahedral phosphate configurations, and the rotation of these moieties may also contribute to the transfer of protons.

In summary, a combination of experimental and modelling techniques has enabled us to gain unique insight into the oxide-ion and proton conduction mechanisms in the gallate $La_{1-x}Ba_{1+x}GaO_{4-x/2}$. These simulations provide a rationalization on the basis of quantitative calculations, as opposed to qualitative arguments, as to the ion-transport mechanisms at the atomic level. Oxide-ion vacancies are shown to be accommodated in the structure through the formation of Ga_2O_7 defects, which are also integral to the mechanism of oxide-ion conduction. In particular, oxide-ion conduction occurs via an unusual cooperative 'cog-wheel'-type process involving the breaking and re-formation of Ga_2O_7 units, as well as the relatively facile rotation of the GaO_4 units. In contrast to the anisotropic oxide-ion conduction mechanism, the proton conduction process is expected to be isotropic. In this case, the rate-determining step has been identified as proton migration around a gallate tetrahedron (intra-tetrahedron), with the activation barrier for transfer between tetrahedra (inter-tetrahedra) being low owing to mediation through hydrogen-bonding interactions. Similar mechanistic aspects may feature in the ionic conduction characteristics of related oxide systems containing tetrahedral moieties.

METHODS

EXPERIMENTAL

$LaBaGaO_4$ and $La_{0.8}Ba_{1.2}GaO_{3.9}$ were synthesized using the solid-state reaction method; stoichiometric amounts of dried La_2O_3, $BaCO_3$ and Ga_2O_3 were intimately ground in a pestle and mortar and fired to 950 °C for 12 h then twice to 1,300 °C for a further 12 h, with intermediate grinding. The 'dry' samples were obtained by slow cooling from 1,000 °C in a dry O_2 atmosphere and then placing the sample directly into a sealed tube. The 'wet' samples were synthesized by heating in H_2O/O_2 and D_2O/O_2 at 500 °C overnight; the samples were removed at temperatures above 100 °C to prevent surface water incorporation.

Structural analysis was carried out using neutron powder diffraction. Time-of-flight neutron diffraction data were recorded on the high-resolution powder diffractometer at the ISIS facility, Rutherford Appleton Laboratory. Data sets from two banks of detectors were used for the refinement; the first was from the backscattering detector bank and the second from the 90° detector bank. Data were collected at room temperature, and all structural refinements were carried out using the General Structure Analysis System suite of programs[14]. The initial refinement of the dry $La_{0.8}Ba_{1.2}GaO_{3.9}$ sample allowed all of the oxygen atoms to be refined freely, and it was observed that only the O3 possessed vacant sites with a very large anisotropic temperature factor. The occupancy for this was therefore set to 0.9 with all of the other oxygen positions fully occupied. From further analysis of the Fourier maps it was observed that there were in fact two regions of nuclear density associated with the O3 position; these were then refined and the total occupancy of both O3 sites was still restrained to 0.9 (see the Supplementary Information).

COMPUTATIONAL

Several computational techniques were used: static lattice and molecular dynamics simulations (based on interatomic potentials) and DFT calculations. Static lattice simulations were carried out using the GULP code[15], with the interatomic interactions represented by ionic pair-wise potentials that include the long-range Coulomb term and an analytical function to model electron-cloud overlap repulsions. The shell model provides an effective description of electronic polarizability. An important feature of these calculations is the modelling of lattice relaxation around the point defect or migrating ion, which was treated by the Mott–Littleton approach[16]. Potential-based molecular dynamics simulations were carried out using the MOLDY code[17]. For the $La_{0.8}Ba_{1.2}GaO_{3.9}$ calculations, the model for the perfect lattice of $LaBaGaO_4$ obtained from static lattice calculations was used with 1/5th of the La randomly replaced with Ba ions and 1/10th of the O3 ions removed. The unit cell was then repeated to form a simulation box of around 2,000 atoms. An initial equilibrium simulation at constant temperature and pressure was carried out, using a time step of 0.002 ps for 10,000 steps. With the obtained average volume, constant temperature and volume simulations were carried out with a time step of 0.002 ps for 75,000 steps (after a further equilibration of 15,000 steps). In this manner, simulations were carried out over a range of temperatures.

Solid-state DFT calculations were carried out using the Plane-Wave Self-Consistent Field program[18]. Core electrons were represented by ultrasoft pseudopotentials[19], and the Perdew–Wang (PW91) density functional[20,21] was used for exchange–correlation. Integration over the Brillouin zone was carried out with $1 \times 2 \times 2$ and $1 \times 1 \times 1$ Monkhorst–Pack grids[22] for calculations on $1 \times 1 \times 1$ and $1 \times 2 \times 2$ supercells of $LaBaGaO_4$, respectively. Cutoff energies of 60 and 180 Rydbergs were used for the plane-wave kinetic energy and charge density respectively, to ensure good convergence of the total energy differences and the calculated structural parameters. The initial unit cell used for geometry optimization was taken from the experimental crystal structure. Calculations of transition states for proton migration were carried out using the NEB method. Intermediate geometries were also generated for proton migration and gallate group rotation to improve the efficiency of the NEB search algorithm. It is worth noting that the atomistic (potential-based) and DFT methods used here have been applied successfully to other ion-conducting oxides[16,23–25].

Received 16 July 2007; accepted 17 September 2007; published 21 October 2007.

References

1. Steele, B. C. H. & Heinzel, A. Materials for fuel-cell technologies. *Nature* **414**, 345–352 (2001).
2. Atkinson, A. *et al.* Advanced anodes for high-temperature fuel cells. *Nature Mater.* **3**, 17–27 (2004).
3. Goodenough, J. B. Oxide-ion electrolytes. *Annu. Rev. Mater. Res.* **33**, 9 (2003).
4. Norby, T. & Larring, Y. Concentration and transport of protons in oxides. *Curr. Opin. Solid State Mater. Sci.* **2**, 593–599 (1997).
5. Kreuer, K. D. Proton-conducting oxides. *Annu. Rev. Mater. Res.* **33**, 333–359 (2003).
6. Iwahara, H. Proton conducting ceramics and their applications. *Solid State Ion.* **86–88**, 9–15 (1996).
7. Haugsrud, R. & Norby, T. Proton conduction in rare-earth ortho-niobates and ortho-tantalates. *Nature Mater.* **5**, 193–196 (2006).
8. Kitamura, N., Amezawa, K. & Tomii, Y. Electrical conduction properties of Sr-doped $LaPO_4$ and $CePO_4$ under oxidizing and reducing conditions. *J. Electrochem. Soc.* **152**, A658–A663 (2005).
9. Li, S., Schönberger, F. & Slater, P. $La_{1-x}Ba_{1+x}GaO_{4-x/2}$: a novel high temperature proton conductor. *Chem. Comm.* **21**, 2694–2695 (2003).
10. Schönberger, F., Kendrick, E., Islam, M. S. & Slater, P. Investigation of proton conduction in $La_{1-x}Ba_{1+x}GaO_{4-x/2}$ and $La_{1-x}S_{r2+x}GaO_{5-x/2}$. *Solid State Ion.* **176**, 2951–2953 (2005).
11. Kendrick, E., Islam, M. S. & Slater, P. R. Developing apatites for solid oxide fuel cells: Insight into structural, transport and doping properties. *J. Mater. Chem.* **17**, 3104–3111 (2007).
12. Kilner, J. A. Optimisation of oxygen ion transport in materials for ceramic membrane devices. *Faraday Discuss.* **134**, 9–15 (2007).
13. Haile, S. M., Boysen, D. A., Chisholm, C. R. I. & Merle, R. B. Solid acids as fuel cell electrolytes. *Nature* **410**, 910–913 (2001).
14. Larson, A. C. & Von Dreele, R. B. "General Structure Analysis System (GSAS)", Los Alamos National Laboratory Report LAUR 86–748 (1994) Toby, B. H. EXPGUI, a graphical user interface for GSAS. *J. Appl. Cryst.* **34**, 210–213 (2001).
15. Gale, J. D. & Rohl, A. L. The general utility lattice program. *Mol. Simul.* **29**, 291–341 (2003).
16. Catlow, C. R. A. (ed.) *Computer Modelling in Inorganic Crystallography* (Academic, San Diego, 1997).
17. Refson, K. Moldy: a portable molecular dynamics simulation program for serial and parallel computers. *Comput. Phys. Commun.* **126**, 309–328 (2000).
18. Baroni, S. *et al.* <http://www.pwscf.org/>.
19. Vanderbilt, D. Soft self-consistent pseudopotentials in a generalized eigenvalue formalism. *Phys. Rev. B* **41**, 7892–7895 (1990).
20. Burke, K., Perdew, J. P. & Wang, Y. in *Electronic Density Functional Theory: Recent Progress and New Directions* (eds Dobson, J. F., Vignale, G. & Das, M. P.) (Plenum, New York, 1998).
21. Perdew, J. P. *et al.* Atoms, molecules, solids, and surfaces: Applications of the generalized gradient approximation for exchange and correlation. *Phys. Rev. B* **46**, 6671–6687 (1992).
22. Monkhorst, H. J. & Pack, J. D. Special points for Brillouin-zone integrations. *Phys. Rev. B* **13**, 5188–5192 (1976).
23. Islam, M. S. Ionic transport in ABO_3 perovskite oxides: a computer modelling tour. *J. Mater. Chem.* **10**, 1027–1038 (2000).
24. Minervini, L., Grimes, R. W. & Sickafus, K. E. Disorder in pyrochlore oxides. *J. Am. Ceram. Soc.* **83**, 1873–1878 (2000).
25. Sayle, T. X. T., Parker, S. C. & Sayle, D. C. Oxygen transport in unreduced, reduced and Rh(III)-doped CeO_2 crystals. *Faraday Discuss.* **134**, 377–397 (2007).

Acknowledgements

This work was supported by the EPSRC (Project grant: GR/S55507/02). We would also like to thank ISIS, Rutherford Appleton Laboratory UK for access to neutron diffraction facilities.
Correspondence and requests for materials should be addressed to P.R.S. or M.S.I.
Supplementary Information accompanies this paper on www.nature.com/naturematerials.